Flue gas injection into depleted tight hydrocarbon reservoirs in the context of global warming mitigation: Computed evolution of some reservoir parameters

Andrey Myagkiy, Claire Pacini-Petitjean, Irina Panfilov, Pranay Morajkar, Pierre Faure-Catteloin, Jacques Pironon, Valérie Burklé-Vitzthum

Flue gas injection into depleted tight hydrocarbon reservoirs in the context of global warming mitigation: computed evolution of some reservoir parameters

Andrey MYAGKIY[1,5], Claire PACINI-PETITJEAN[2,3], Irina PANFILOVA[1], Pranay MORAJKAR[4,6], Pierre FAURE-CATTELOIN[3], Jacques PIRONON[2], Valérie BURKLE-VITZTHUM[4]*

[1] Université de Lorraine, CNRS, LEMTA, F-54505, Vandoeuvre-lès-Nancy, France

[2] Université de Lorraine, CNRS, Georessources, F-54500, Vandoeuvre-lès-Nancy, France

[3] Université de Lorraine, CNRS, LIEC, F-54500, Vandoeuvre-lès-Nancy, France

[4] Université de Lorraine, CNRS, LRGP, F-54000, Nancy, France

[5] Storengy, Bois-Colombes, France

[6] School of Chemical Sciences, Goa University, Taleigao Plateau, 403206, Goa, India

Corresponding author*: valerie.vitzthum@univ-lorraine.fr (Valérie BURKLE-VITZTHUM – LRGP 1 rue Granville 54001 Nancy Cedex - France)

Keywords: depleted oil reservoir, CO_2 storage, temperature profile, oxy-combustion, CFD

Abstract:

CO_2 storage in depleted tight hydrocarbon reservoir seems to be a promising solution to mitigate greenhouse gas emissions. However, flue gas contains not only CO_2 but also minor gaseous impurities due to CO_2 production or capture processes. In the case of oxy-combustion, the main impurity can be O_2 in concentration up to 7 %. O_2 injection into the reservoir can lead to the oxidation of the residual hydrocarbons and therefore, it is necessary to assess the thermal consequences on the reservoir.

COMSOL Multiphysics® has been used to model an axisymmetric fractured porous reservoir with its cap and base rocks and containing *n*-octane as a model compound of residual oil. A global kinetic model for *n*-octane oxidation has been derived from a previous detailed free-radical model, and implemented into the reservoir model. Simulated injections of N_2/O_2 mixture (representing a simplified flue gas) have been performed to compute temperature, pressure and *n*-octane concentration profiles. The results show that the oxidation exothermicity may have a strong influence on temperature profile, especially when the heat capacity of the rock is rather low. In these conditions, the remaining hydrocarbons may be consumed in some months. However, the influence of the thermal conductivity seems negligible. Therefore, it appears safer to select reservoirs whose rocks compositions, in particular the cap and base rocks, have a high heat capacity to promote heat dissipation. It is a criterion to consider when selecting a storage site containing residual hydrocarbons, especially for CO_2 captured after oxy-combustion.

1. Introduction

The CO_2 emissions from combustion of fossil fuel is still increasing and reached 33.62 Giga ton/year in 2019 (IEA, 2022), leading to dramatic climate warming due to CO_2 greenhouse gas effect (IPCC, 2021).

The mitigation of such alarmingly increasing CO_2 emissions mainly considers three combined strategies: 1) switching to a low-carbon economy which relies on renewable and alternative energy sources; 2) increasing the efficiency of the current technologies and decreasing the energy loss; 3) using CCS (Carbon Capture and Storage) technologies to reduce CO_2 emissions, since the worldwide dependency on fossil fuels is probably going to last several more decades (Maroto-Valer, 2010). CCS appears to be an efficient strategy to mitigate anthropogenic CO_2 emissions from large sources, by up to 90% (Maroto-Valer, 2010). CCS mainly consists of: 1) capturing and potentially separating CO_2 from the other exhaust gases; 2) carrying CO_2 to its storage location, after compression to supercritical conditions; 3) storing CO_2, e.g. in several types of geological storage sites (Liu et al., 2018).

The geological reservoirs that are the most frequently considered are the deep saline aquifers. They may be subjected to regional pressure build-up due to water movement, which may affect the reservoir integrity (Hamza et al. 2021) and the storage capacities. Injecting CO_2 into coal seam reservoirs is also considered, potentially for EMR (Enhanced Methane Recovery) purpose (Zhang and Ranjith, 2019). Another type of geological reservoir that is the focus of attention, is the depleted hydrocarbon (gas or oil) reservoirs. Their storage capacity is much higher than that of coal seams (Kaldi et al., 2009) and they present several advantages over saline aquifers. Indeed, the oil and gas fields have proved their potential containment by the retention of hydrocarbons for millions of years. They have been widely studied (storage capacity, structural and stratigraphic patterns...) (Kaldi et al., 2009). Another advantage is the limited pressure inside the reservoirs due to the former hydrocarbon production, which allows injecting CO_2 at moderate pressure, which is technically and economically favorable.

Power plants and other industrial processes that use combustion usually produce flue gases at approximately atmospheric pressure, with CO_2 diluted mostly in N_2. CO_2 must then be separated from other components in the flue gas (post-combustion capture). Another solution is pre-combustion which consists of the removal of carbon from the fuel prior to combustion. At last, oxy-combustion, i.e. combustion in purified O_2 instead of air, is another way to solve this issue. Oxy-combustion enables a much easier capture of CO_2 by the flue gas condensation than post-combustion in which N_2 is the dominant component (Tumsa et al., 2017). Nevertheless, flue gas from oxy-combustion may contain a relatively high level of impurities, such as water, Ar (0-5%), N_2 (0-15%), O_2 (0-7%) and SO_2 (0-1.5%) (Mikunda, 2012).

This study focuses on CO_2 captured after oxy-combustion processes, which contains residual O_2. It aims to assess some effects of the presence of O_2 in the injected gas on some parameters of the gas/oil depleted reservoir and to assess if it is necessary to remove O_2 before injection since purification is expensive. Previous studies already showed that the impurities reduce the structural trapping capacity

for CO_2 by reducing the CO_2 density (Wang et al., 2012). Another consequence of the presence of O_2 is examined here. Indeed our previous studies (Pacini-Petitjean et al., 2015a, 2015b, 2016) showed that the oxidation of the hydrocarbons occurs in the temperature conditions of relatively deep hydrocarbon reservoirs (T > 373 K). Therefore, the oxidation kinetics of the residual hydrocarbons may impact on the pressure and temperature evolution in the reservoir during the injection and storage. That is why a model of one part of a fractured porous reservoir has been setup by COMSOL Multiphysics® (version 5.6), which considers heat and mass transfers, flow and kinetics. Several assumptions have been made, in particular the flue gas has been replaced by air to emphasize the oxidation phenomenon and to stay in the same conditions as in our previous studies. The other impurities have not been considered. This simplified representation of a flue gas appears appropriate since the study mainly concerns the thermal effects of O_2. An injection well in the center and perforated over the entire height of the reservoir has been considered. The model aims at computing the consumption of O_2 and the hydrocarbons, the pressure increase and the temperature evolution as a function of time, throughout the part of the reservoir considered. Since the temperature appears to be a key parameter for a safe storage, the influence of the thermal properties (heat capacity and thermal conductivity) of the rocks are also addressed. Although a tight reservoir is considered here, this study could also be valuable for EOR (Enhanced Oil Recovery) modelling (Ahmadi et al., 2016) or modelling of the combination of EOR and CO_2 storage (Bender and Akin, 2017).

2. Materials and methods

2.1. Modelling tools

The Computational Fluid Dynamics modelling has been performed by COMSOL Multiphysics® (version 5.6). The different steps of the modelling are described below. A detailed kinetic model for *n*-octane oxidation (Pacini-Petitjean et al., 2015b) has been used in order to derive accurate kinetic parameters

to be implemented in COMSOL Multiphysics. The computations of the kinetic model have been performed by CHEMKIN II using the code SENKIN in a closed isochoric reactor (Kee et al., 1989).

2.2. Geological context and rock characteristics

The geological structure considered is a deep, isolated, faulted Jurassic horst, overlaid by a 4500 m thick overburden series of turbiditic flysch deposits of Upper Cretaceous (Cenomanian) to Tertiary (Eocene) age, and situated within the Pyrenean foredeep basin. The analysis of cored materials led to the mineralogical composition of the cap-rocks (Table 1) and the reservoir (Table 2) (Girard et al., 2013). The composition of the reservoir varies because of the mineralogical heterogeneity of such a fractured reservoir. It has been assumed that the injection of CO_2 does not modify the mineralogical composition of the rocks, which remains constant throughout the study, as well as the porosity and permeability of the rocks. The mineralogical and geochemical impact of gas impurity injection in the same geological environment have been tested by Renard et al. (2014).

Table 1. Mineralogical composition of the cap-rocks.

Mineral	**Mass fraction %**
Pyrite	0.3
Ankerite	4.6
Fe Dolomite	0.0
Non-Fe Dolomite	2.1
Calcite	63.2
Quartz	10.5
Illite	8.3
Interstratified clays	6.5

Table 2. Mineralogical composition of the reservoir.

Mineral	**Range mass fraction %**	**Average mass fraction %**
Dolomite	84-98	93.5
Calcite	0-4	0.5
Quartz	1-4	2.5
Pyrite	0-2	0.4
Illite	1-5	2.5
Chlorite	0-1	0.3
Apatite	0-1	0.2
Insoluble Organic Matter	<<1	0.1

According to the mineralogical composition, Calcite and Quartz are the major minerals in the cap-rock and the reservoir is mainly made of Dolomite. The other minerals were neglected for the study. Table 3 sums up the thermal properties of these three minerals (heat capacity and thermal conductivity) (Birch and Clark, 1940; Krupka et al., 1985).

Table 3. Heat capacitiy (C_p) and thermal conductivity (K) of the major minerals of cap-rocks and reservoir (Birch and Clark, 1940; Krupka et al., 1985).

Mineral	**Highest C_p ($J.kg^{-1}.K^{-1}$)**	**T(K)**	**Lowest C_p ($J.kg^{-1}.K^{-1}$)**	**T(K)**	**Highest K ($W.m^{-1}.K^{-1}$)**	**T(K)**	**Lowest K ($W.m^{-1}.K^{-1}$)**	**T(K)**
Dolomite	1188	620	933	350	4.98	273	2.55	573
Quartz	1163	925	319	115	6.19	1400	1.34	280
Calcite	1289	1200	807	293	4	273	2.13	600

Since the dolomite is the main rock of the reservoir and since the heat capacity of dolomite does not depend a lot on temperature in the considered temperature range (Supplementary material), the heat capacity of the reservoir has been considered as constant and equal to 933 $J.kg^{-1}.K^{-1}$ (Table 3). For the cap-rocks, by considering only the main minerals, the mean heat capacity is from the same order of magnitude and does not change a lot with temperature as well. So, to simplify, the heat capacity of the base and cap-rocks has been taken constant and equal to 933 $J.kg^{-1}.K^{-1}$ too.

For the CFD modelling, the thermal conductivity has to be expressed as a function of temperature, since it depends a lot on temperature (Table 3). An equation as eq (1) is usually used.

$$K = \sum a_i \times T^{ni} \qquad \text{eq (1)}$$

Where T is the temperature (K) and a_i and n_i are coefficients, positive or negative.

The equations used in this study are given in the Supplementary Material.

The thermal conductivity of the reservoir and cap rocks was estimated by eq (2).

$$K\ (bulk) = \sum_{i=1}^{n} K_i M_i / M_{tot} \qquad \text{eq (2)}$$

Where M_i , K_i are respectively the mass and thermal conductivity of component *i* of the rocks, and M_{tot} is the total mass of the bulk material. According to the previous equations, the thermal conductivity of the cap and base rocks varies between 3.35 and 4.95 $W.m^{-1}.K^{-1}$, and the thermal conductivity of the reservoir rocks from 3.65 to 5.45 $W.m^{-1}.K^{-1}$, in the studied conditions, when the temperature increases.

The part of the reservoir considered has been modelled by a cylinder (diameter: 800 m; thickness: 200 m), covered by 100 m of cap rock and lying on 100 m of base rock with the same properties as the cap-rock (Figure 1). The injection well is supposed to be in the center and perforated over the entire height

146 of the reservoir. It is surrounded by several injection wells in which the injection flow rates are the
147 same. So, the drainage zone considered is surrounded by the drainage zones of the other wells and it
148 seems separated from the other drainage zones by impermeable boundaries. These boundaries act as
149 tight walls since the composition and temperature are the same on both sides and so no heat or mass
150 transfer is possible. Therefore, the model is radial and axisymmetric and the cylinder has been
151 considered as tight and thermally insulated on the sides.

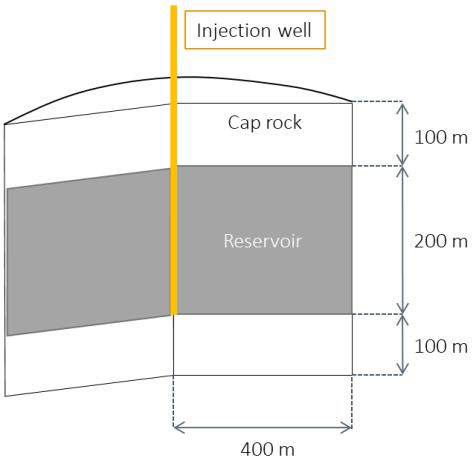

152

153 **Figure 1.** Axisymmetric modelling of the geological pile considering homogeneous cap-rock and base-
154 rock of 100 m, and a heterogeneous part of a reservoir of 200 m of thickness.

155

156 *2.3. Modelling of the reservoir fractured medium*

157 The reservoir is considered as a fractured porous medium, *i.e.* a medium intersected by a network of
158 interconnected fractures. The fluid flows in the fractures as well as in the matrix blocks. These two
159 superposed continua coexist and interact with each other.

160 Another approach to model this system is to use effective parameters for porosity and permeability
161 (Table 4) without dividing the porous media into matrix blocks and fractures.

162

163 **Table 4**. Effective porosity and permeability of reservoir rocks (unpublished data).

Conduction properties	Effective
Porosity	3%
Permeability	1 mD

Since the fluid flows more rapidly in the fractures than in the matrix, it has been assumed that it does not directly flow from one block to another. First it flows from a block into the fractures, and then into another block or it remains in the fractures (Arbogast et al., 1990). Therefore, the equations that describe the flow in the fracture continuum contain a source term that represents the flow of fluid from the matrix to the fractures. This term is considered as being distributed over the entire medium. Finally, we have assumed that the external sources and sinks interact only with the fracture system, since the flow is much faster in this system than in the matrix blocks. Based on these assumptions, the mass conservation of the flow through the matrix and fractures in a fractured porous medium is given by eq (3-4).

$$\frac{\partial(\rho\,\phi_m)}{\partial t} + \mathrm{div}(\rho\vec{v}_m) = q_{mf} \qquad \text{eq (3)}$$

$$\frac{\partial(\rho\,\phi_f)}{\partial t} + \mathrm{div}\left(\rho\,\vec{v}_f\right) = -q_{mf} + q_{ext} \qquad \text{eq (4)}$$

Where the subscripts *m* and *f* represent the matrix and fracture continua respectively, ϕ stands for the porosity, $\vec{v}$ for the velocity, ρ for the density, q_{mf} denotes the flow from the matrix to the fractures, q_{ext} indicates the external sources and sinks. The velocities $\vec{v}_m$ and $\vec{v}_f$ are determined by Darcy's law.

Since in this study the effective parameters were used for the gas multicomponent system behavior in fractured media, eq (5) and (6) have to be considered instead of eq (3) and (4).

$$\phi_{ef}\frac{\partial(\rho\, C_i)}{\partial t} + \mathrm{div}(\rho C_i \vec{v}) = D^i - S^i \qquad \text{eq (5)}$$

$$\vec{v} = -\frac{k_{ef}}{\eta}(\overrightarrow{\mathrm{grad}}\, P + \rho g) \qquad \text{eq (6)}$$

ϕ_{ef}, k_{ef} are the effective porosity and permeability respectively, η is the fluid dynamic viscosity, P is the pressure, C_i is the molar concentration of species *i*, ρ is the gas density and D^i, S^i schematically represent diffusion and source terms respectively. These terms are detailed below.

Furthermore, we assume that porosity does not change during the simulations, as explained below.

2.4. Governing equations

The equations that describe a reacting single-phase gaseous flow in a porous medium are detailed in this sub-section. It is assumed that the gas is ideal.

Eq (7) corresponds to the energy equation.

$$C_p\frac{\partial T}{\partial t} + \vec{v}\, C_{pg}\, \rho_g\, grad(T) = div\big(K_T\, grad(T)\big) + Q \qquad \text{eq (7)}$$

with

$$C_p = \phi_{ef} C_{pg}\rho_g + \big(1-\phi_{ef}\big)C_{ps}\rho_s \ , \qquad K_T = \phi_{ef}K_g + \big(1-\phi_{ef}\big)K_s$$

where C_{pg} and C_{ps} are specific heat capacity of gas and solid rock respectively, K_g and K_s are thermal conductivity of fluid and rocks, ρ_g is fluid density, ρ_s is rock density. Q stands for the volumetric power released by the fuel oxidation. It is given by eq (8).

$$Q = H \times W \qquad \text{eq (8)}$$

where *H* is the enthalpy of reaction and *W* the rate of the chemical reaction. These terms are detailed below, in a specific subsection.

The mass conservation equation of the species *i* (*n*-octane, oxygen, nitrogen or products) describing the chemical reaction in single gas phase is written as eq (9).

$$\Phi_{ef}\frac{\partial(\rho_g C_i)}{\partial t} + \mathrm{div}\left(\rho_g C_i \vec{v}\right) = \Phi_{ef} div\left(\rho_g \vec{J_i}\right) - \rho_g^0 W_i \qquad \text{eq (9)}$$

Where $\vec{J_i}$ is the molar flux of species *i*, ρ_g^0–the gas density at initial conditions and W_i the rate of production or consumption of *i* component with consideration of its mass-weighted stoichiometric coefficient (Yucel Akkutlu and Yortsos, 2003).

The velocity of the flow is deduced from the Darcy's law (eq (6)), assuming that the fluid is mostly composed of nitrogen. Nitrogen viscosity is given as a function of temperature in the Supplementary material.

The gradient of pressure in the reservoir is described by the diffusion-type equation eq (10) (Monteiro et al., 2012).

$$\Phi_{ef}\frac{\partial \rho}{\partial t} = \mathrm{div}\left(\frac{k_{ef}}{\eta}\rho\,\overrightarrow{\mathrm{grad}P}\right) \qquad \text{eq (10)}$$

The system of the equations (7)-(10) should be completed by the equation of state for gas and porous media. The density of gas can be found as follows (eq (11)):

$$\rho_g = M_g\frac{P}{z(P)R\,T}, \qquad \text{eq (11)}$$

where P is the pressure, T is the temperature, R is the universal gas constant, $z(P)$ is the gas compressibility, and M_g the average molecular weight of the gas. We assume that the equation of state for the gas phase is the ideal gas law, thus z=1.

225 The porous medium is considered to be low deformable. In comparison with the gas compressibility,
226 the compressibility of rocks can be neglected. The permeability of porous rocks is also assumed as
227 constant. Moreover, the potential cooling of the injected gas by the Joule-Thomson effect has been
228 considered as negligible since the pores are very small.

229 *2.5. Kinetic modelling*

230 It has been assumed that the hydrocarbons remaining in the depleted reservoir can be modelled
231 considering a single hydrocarbon skeleton of an average chain-length (such as *n*-octane), and that the
232 fluid does not contain any water, except the product of the oxidation.

233 All effects of the injection on the reservoir properties (composition, porosity, ...) and the exothermicity
234 of the oxidation reactions of the reservoir rocks have been neglected, since there was no water initially
235 contained in the reservoir and the production of water is rather low (Pacini-Petitjean et al., 2016).
236 Indeed, all reactions of the rocks with the injected gas requiring water (Renard et al., 2014), they have
237 not been considered in this study.

238 It has been previously demonstrated (Pacini-Petitjean et al. 2015a) that CO_2 does not react with the
239 hydrocarbons in the reservoir conditions. Therefore, CO_2 has been replaced by N_2 in this study, as in
240 the previous studies (Pacini-Petitjean et al. 2015a, 2015b and 2016), though their thermal and flow
241 properties could slightly modify the quantitative results. Although the molar fraction of O_2 remaining
242 after oxy-combustion is usually less than 6%, as for in the previous experimental studies, the air
243 composition was used to simulate the injected gas. Indeed, Pacini-Petitjean (2015) compared the
244 experimental results of *n*-octane oxidation with 3% and 20% of O_2, and got the same consumption
245 kinetics of *n*-octane, which is due to the large excess of O_2 in comparison to *n*-octane. So, to be
246 consistent with our previous studies, air has been considered for the injection as a model of flue gas.

247 In a previous study (Pacini-Petitjean et al., 2015b), a detailed kinetic model for *n*-octane oxidation was
248 built, which includes more than 3000 free-radical reactions. Due to the size of the model, it is not
249 possible to implement the full mechanism into COMSOL Multiphysics software. Therefore, a single

reaction has been implemented in the software, that is the total oxidation of *n*-octane (eq (12)), and a very simple kinetic law was used in this study. Oxygen is present in large excess in comparison to *n*-octane, since the injection of gas is continuous until the limit value is reached and the molar fraction of *n*-octane drops not only by oxidation, but also by dilution in the injected gas stream. In these conditions, it has been considered that the kinetic law does not depend on oxygen concentration, but only on *n*-octane concentration. It has been observed that a kinetic order of 2 fits *n*-octane consumption satisfactorily (eq (13)) (Figure S1). Using the kinetic model in other conditions than a large excess of O_2 compared to *n*-octane would lead to totally erroneous conclusions.

$$C_8H_{18} + \frac{25}{2}O_2 \rightarrow 8\,CO_2 + 9H_2O \qquad \text{eq (12)}$$

$$W = A \times e^{-E_a/RT} \times C_{octane}^2 \qquad \text{eq (13)}$$

It must be noted that, according to a previous study (Pacini-Petitjean et al., 2016), the production of water and CO_2 is rather slow and low, and that the intermediary products (ketones and carboxylic acids) are predominant. That is why the potential effect of water and CO_2 on the phase state or the fluid properties has not been considered in this study. It also means that eq (12) is a rough equation of reaction, but what really matters in this study is the kinetics of *n*-octane consumption and the heat release.

Concerning the kinetic parameters, the best match with CHEMKIN data has been obtained with A = 2.3×10^6 $m^3.mol^{-1}.s^{-1}$ and E_a = 100 kJ/mol, where A is the frequency factor and E_a the activation energy (Figure S1).

The enthalpy of reaction is of the utmost importance in this study, in order to be able to estimate the temperature evolution in the reservoir. First, it has been assumed that the heat release is only related to the enthalpy of total *n*-octane oxidation (eq (12)), and that it is constant and equal to - 5112.6 kJ/mol (Turns, 2012, value at 298 K). The influence of temperature on the evolution of the enthalpy of reaction has been neglected. Nevertheless, the reaction is much more complex than a single reaction and the

enthalpy of reaction varies according to the evolution of main reaction pathways. Therefore, the volumetric power released (eq (8)) was directly computed as a function of *n*-octane concentration, using CHEMKIN. Then, the curve obtained was fitted by a polynomial function in order to be used directly in COMSOL Multiphysics (Supplementary material).

2.6. Initial and boundary conditions

In the model, the initial temperature of the top of the reservoir was set to 423.15 K, which corresponds to a rather hot and deep reservoir, and the initial Bottom Hole Pressure (BHP) to 30 bar, characteristic of a depleted reservoir. The temperature changes with depth are considered by a geothermal gradient of 30°C/km. The initial molar fraction of *n*-octane was taken equal to 0.015 in the entire reservoir, the rest being nitrogen.

In the well, the BHP was set to 100 bar and maintained constant during the entire injection. That means that the mass flow rate of the injected gas decreases during the process. The molar fractions of oxygen and nitrogen were taken equal to 0.22 and 0.78 respectively, as in our previous studies (Pacini-Petitjean et al. 2015a, 2015b and 2016). It has been considered that the injection lasts until the pressure reaches 100 bar in the entire reservoir.

The boundary conditions set in this study correspond to the Neumann conditions, which means that there is no heat flux or fluid flow across the boundaries (eq (14)).

$$\begin{cases} \vec{n} \cdot \left(K_{ef} \vec{\nabla} T\right) = 0 \\ \vec{n} \cdot \left(D_i \vec{\nabla} C_i\right) = 0 \end{cases} \qquad \text{eq (14)}$$

Where $\vec{n}$ is a vector normal to the wall.

The thermal reservoir models account for heat exchange with the surroundings, typically through heat conduction to the cap and base rocks. The insulated walls are shown in Figure 2. As explained before, the sides are considered as insulated walls, because the drainage zone is surrounded by other drainage

297 zones leading to symmetrical temperature profiles and so to the same temperature on both sides. On
298 the other hand, it has been assumed that the fluid does not penetrate into the cap or the base rocks.

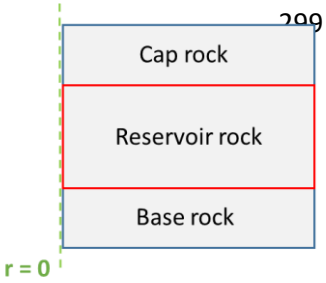

300

301 **Figure 2.** Walls in blue are thermal insulated, and walls in red prevent the fluid flux. Dashed green line
302 corresponds to the well location.

303 ## 3. Results and discussion

304

305 ### *3.1. Simulations at constant enthalpy of reaction*

306 The temperature and *n*-octane concentration in the entire reservoir have been computed up to about
307 10 years. For an example, Figure 3 shows the results after 1500 days (about 4 years) along a cut-line.
308 Near the well, in the first 20 m, almost all *n*-octane is consumed and the consumption of *n*-octane has
309 begun in the entire reservoir. The temperature increases in less than half of the reservoir's radius, but
310 the increase is less than 10 K. The maximum temperature is reached after 2500 days (almost 7 years –
311 end of injection) and it is equal to 443 K. The temperature profile is represented in Figure 4. The
312 maximum temperature is approximately located at 200 m of the injection well (radial position) and
313 half height. The temperature of the cap and base rocks have also increased by thermal conduction.
314 After 2500 days, the pressure reaches 100 bar and so no more gas is injected. It should be noted that
315 the auto-ignition temperature of *n*-octane is 493 K (De Soete and Feugier, 1976), which means that
316 there is apparently no auto-ignition in the reservoir in the studied conditions.

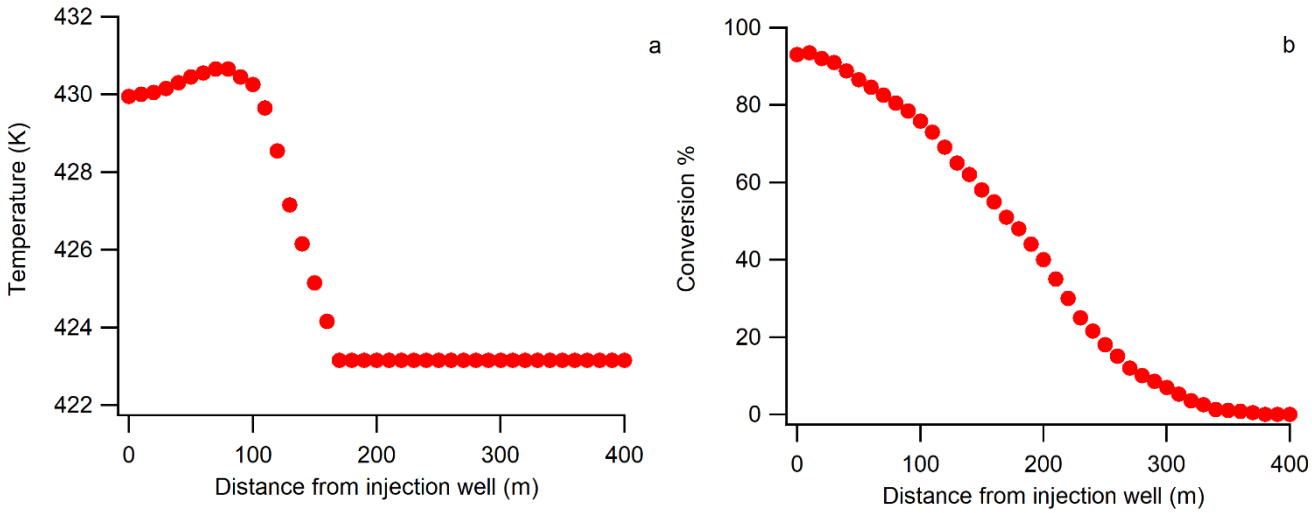

Figure 3. Temperature (a) and *n*-octane conversion (b) as a function of the distance from injection well, after 1500 days (cross-sections) – constant enthalpy of reaction (end of injection: 2500 days – $C_{p\ rocks}$ = 933 $J.kg^{-1}.K^{-1}$).

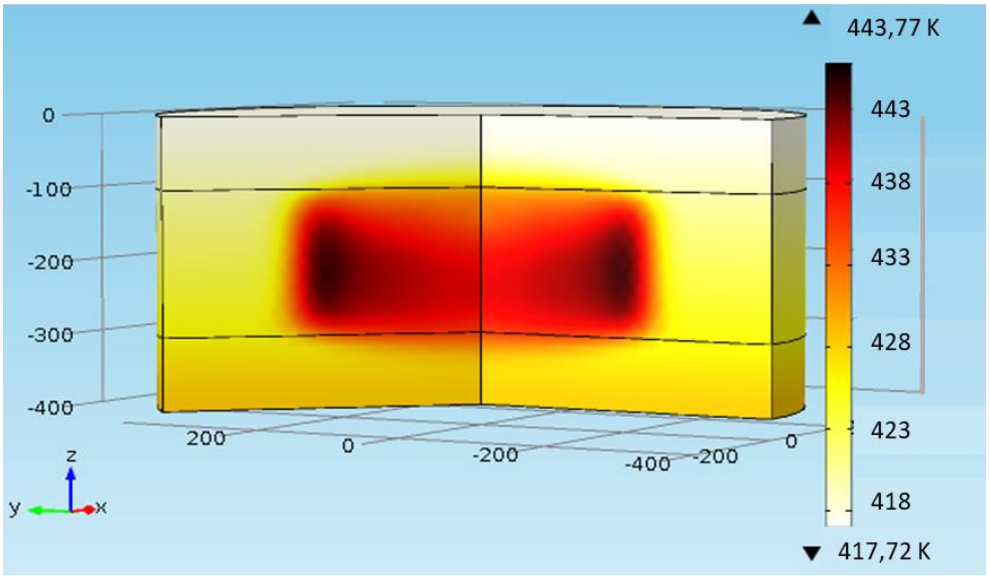

Figure 4. Temperature profile in the reservoir (between -100 and -300 m), in the cap rock (between 0 and -100 m) and in the base rock (between -300 and -400 m), after 2500 days (end of injection – $C_{p\ rocks}$ = 933 $J.kg^{-1}.K^{-1}$).

3.2. Simulations with the heat release estimated from CHEMKIN results

In this subsection, the reservoir temperature has been computed using the volumetric power release estimated from CHEMKIN as a function of remaining *n*-octane concentration. The temperature increases much faster than in the previous computation (Figures 5a and b) and reaches 533 K in the center of the reservoir after only 60 days, which is above the auto-ignition temperature. Figure 6 shows the temperature evolution as a function of time and radial position in a cross section and so the reaction wave can be observed. The heat transfer by the rocks is much slower than by the fluid, so the cap and base rocks warm up very slowly. According to Figure 7a, *n*-octane is reduced to half of the initial value of the reservoir after 50 days. Figure 7b shows the progression of oxygen into the reservoir. After the total consumption of *n*-octane, the dissipation of heat in the base and cap rocks can be observed (Kihm et al., 2019) and the temperature slowly decreases and is almost uniform in the reservoir and equal to 480 K after 500 days (Figure 5c).

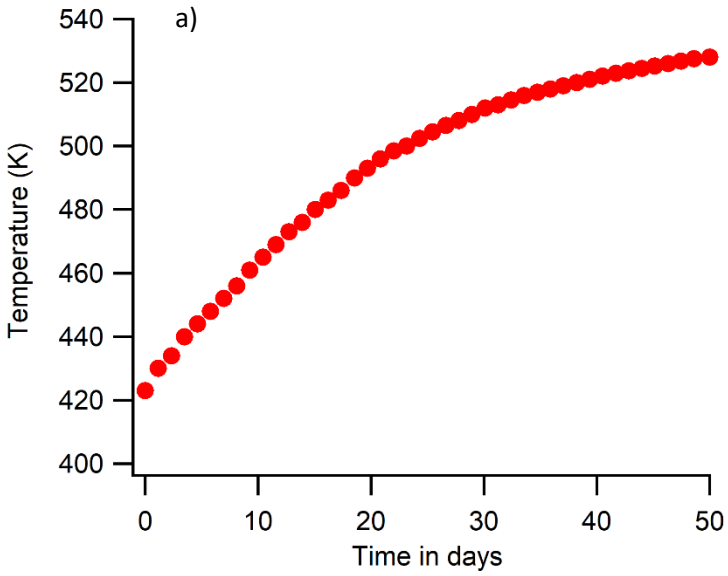

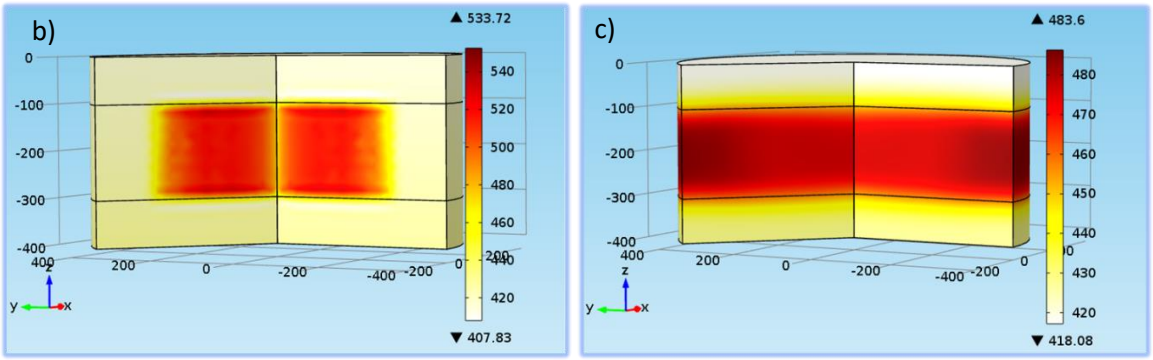

Figure 5. a) Average temperature in the reservoir as a function of time until 50 days; b) Temperature profile in the reservoir after 50 days; c) Temperature profile in the reservoir after 500 days (end of injection: 300 days– $C_{p\ rocks}$ = 933 J.kg^{-1}.K^{-1}).

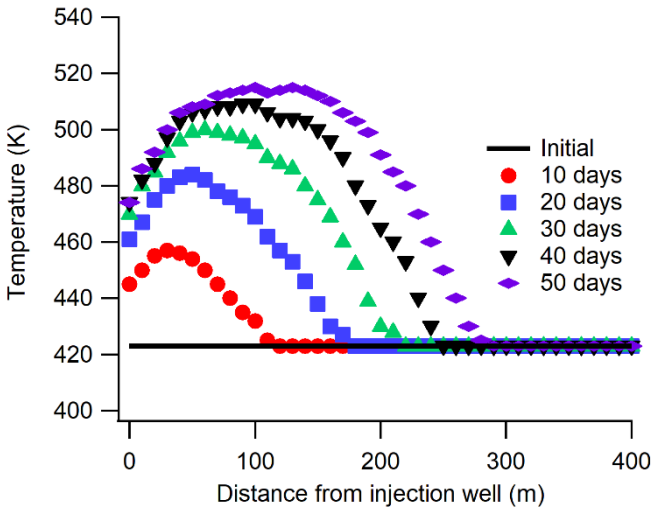

Figure 6. Temperature as a function of the distance from injection well (cross-sections after 10, 20, 30, 40 and 50 days) – heat release from CHEMKIN results (end of injection: 300 days– $C_{p\ rocks}$ = 933 J.kg^{-1}.K^{-1}).

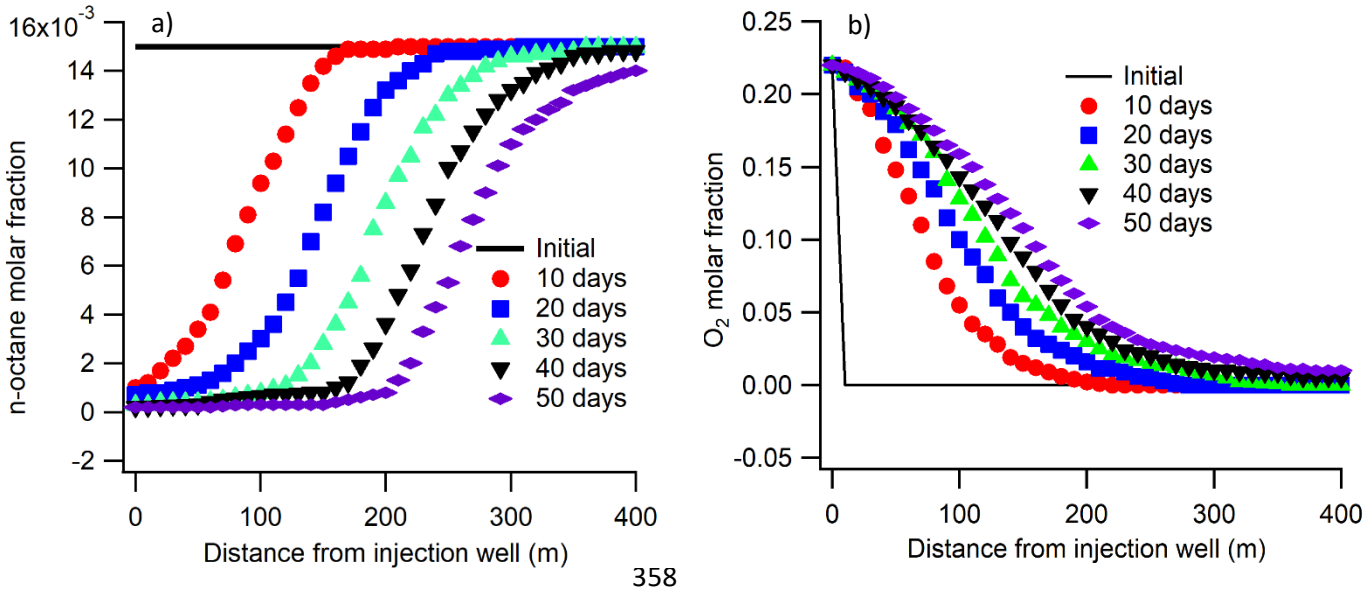

358

359 **Figure 7.** Molar fractions (gas phase) of the reactants (a, *n*-octane and b, O_2) as a function of the
360 distance from injection well (cross-sections after 10, 20, 30, 40 and 50 days - end of injection: 300
361 days– $C_{p\ rocks}$ = 933 $J.kg^{-1}.K^{-1}$).

362 Figure 8a shows the pressure profile after 50 days. Pressure reaches 80 bar near the injection well. The
363 average pressure reaches 100 bar after almost one year (300 days - Figure 8b), which corresponds to
364 the end of the gas injection into the well in the simulations. Indeed, the temperature increase is greater
365 and faster with the heat release estimated from CHEMKIN results than with a constant enthalpy of
366 reaction, and so the pressure limit is reached sooner than by the first simulations. In the meantime,
367 the oxygen concentration slowly stabilizes.

368

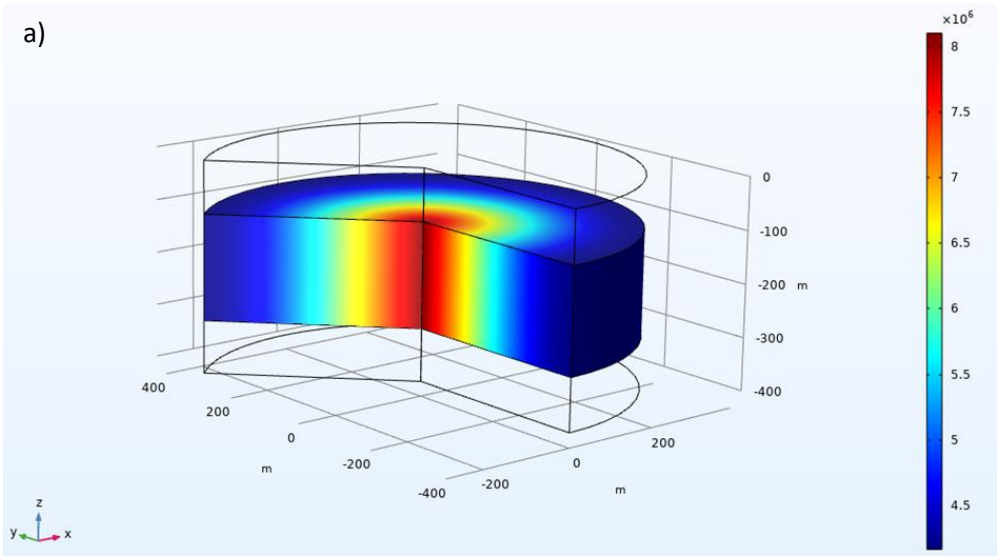

369

370

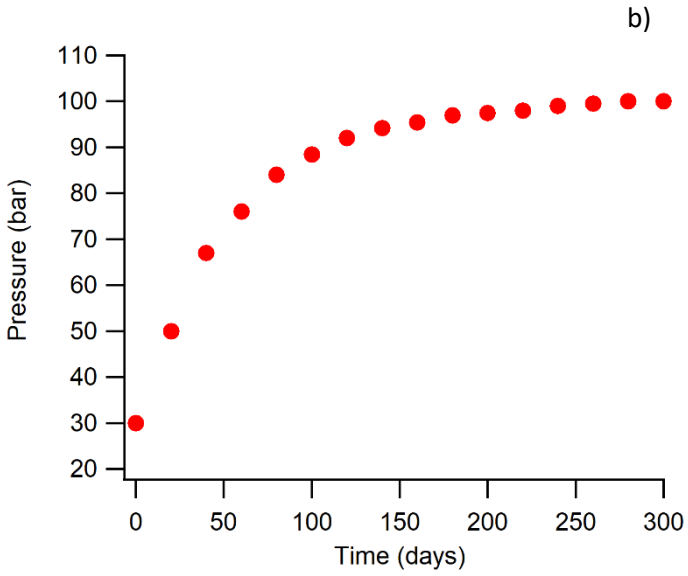

371

372 **Figure 8.** a) Pressure (bar) profile in the reservoir 50 days after the beginning of the injection; b)
373 Average pressure in the entire reservoir as a function of time (end of injection: 300 days– $C_{p\ rocks}$ = 933
374 $J.kg^{-1}.K^{-1}$).

375

376 According to this study, which considers the heat released in a more realistic way than only the
377 enthalpy of total oxidation, the gas injection into the reservoir would strongly affect the hydrocarbon
378 composition and the temperature over a few months after the beginning of the injection.

379 Nevertheless, the reactivity of *n*-octane against oxidation was estimated in homogeneous phase. The
380 reactivity in a porous medium could be lowered by the recombination of the radicals onto the walls
381 (Garo et al. 1984). The heat release and the reaction rate would be lower than estimated here.
382 Moreover, the temperature increase depends on the competition between the kinetics of oxidation
383 and the thermal properties of the rocks, which is studied in the next sub-section.

384

385 *3.3. Influence of thermal properties anisotropy on heat dissipation into the reservoir*

386 The evolution of temperature in the reservoir is governed by the competition between the
387 exothermicity of reaction, the dynamics of the gas injected and the thermal properties of the reservoir,
388 the cap and the base rocks. In order to assess the influence of anisotropy in thermal conductivity on
389 heat dissipation, first, a horizontal thermal conductivity 10 times higher than the vertical one was set
390 in the simulations (Figure 9). The opposite situation was also considered (Figure 9). The maximum
391 temperature is reached after 80 days and is about 540 K in both cases. No major difference is observed,
392 but the slope after the maximum temperature point in the case of a higher vertical conductivity than
393 the horizontal one. It could be explained by the higher vertical conductivity, which leads to more
394 thermal diffusion into the cap and base rocks. Nevertheless, the thermal conductivity of the rocks has
395 only a small influence in comparison with the dynamics of the gas injected and the heat released by
396 the oxidation.

397

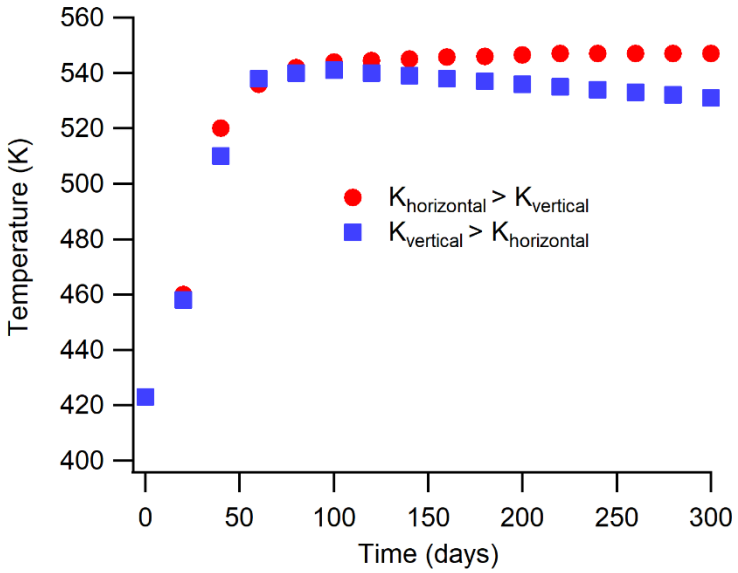

Figure 9. Temperature as a function of time in case of anisotropy (red circle markers: horizontal thermal conductivity 10 times higher than the vertical one; blue square markers: opposite situation - end of injection: 300 days– $C_{p\ rocks}$ = 933 J.kg^{-1}.K^{-1}).

Secondly, the influence of the heat capacity of the reservoir rock was considered. The heat capacity of usual reservoir rocks ranges from 500 to 1500 J.kg^{-1}.K^{-1}, depending on mineral composition. These two limit cases were successively investigated. First, the heat capacity of the reservoir, cap and base rocks was set to 500 J.kg^{-1}.K^{-1}. In this case, the rocks warm up very quickly (Figure 10). The reservoir temperature reaches its maximum (about 570 K) after 40 days, and then the temperature slightly decreases. After 100 days, the temperature in about three quarters of the reservoir is greater than 530 K.

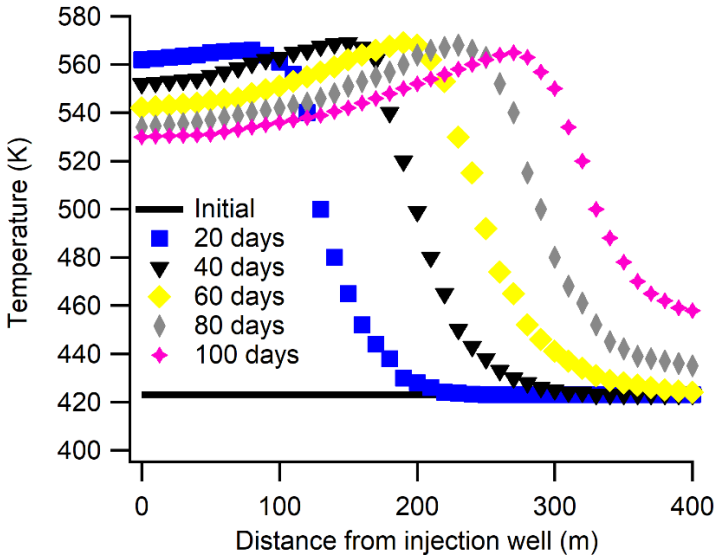

410

411 **Figure 10.** Temperature as a function of time and distance from the injection well (heat capacity of the

412 reservoir, cap and base rocks set to 500 $J.kg^{-1}.K^{-1}$- end of injection: 300 days).

413

414 Secondly, the heat capacity was set to 1500 $J.kg^{-1}.K^{-1}$ (Figure 11). In this situation, since the rocks absorb

415 most of the energy released by the exothermicity of the reactions, the temperature only increases by

416 3 K after 100 days, which is completely negligible. Figure S2 compares the evolution of temperature

417 computed for the three heat capacities tested in order to better highlight their influence. As expected,

418 the consumption of the reactants is all the faster than the heat capacity is lower and the temperature

419 higher, since the kinetics is temperature dependent (Figure 12). Figures S3 and S4 compare the

420 evolution of respectively *n*-octane and O_2 molar fractions computed for the three heat capacities. The

421 difference between the results obtained with 500 and 933 $J.kg^{-1}.K^{-1}$ is more pronounced than between

422 933 and 1500 $J.kg^{-1}.K^{-1}$ since the increase of temperature with 500 $J.kg^{-1}.K^{-1}$ is very important. It appears

423 that there is no major difference between 933 and 1500 $J.kg^{-1}.K^{-1}$ except at the very beginning of the

424 injection. In the case of O_2, since it is progressively injected into the reservoir, the concentration

425 increases faster when the heat capacity is high. As O_2 is less consumed at low temperature, which

426 corresponds to a high heat capacity, it penetrates the reservoir faster.

427

Contrary to the thermal conductivity, the heat capacity has a major influence on temperature in the reservoir. In order to choose the location of the storage site, which ensures the maximum thermal stability of the reservoir, it is particularly important to pay attention to the heat capacity of the reservoir, base and cap rocks and to choose rocks with the highest heat capacity. Furthermore, for a given depleted reservoir, it is important to adapt to the thermal characteristics of the reservoir and to the remaining hydrocarbons, the composition of the injected gas, its flow rate, and the temperature and the pressure in the well, in order to limit the risk.

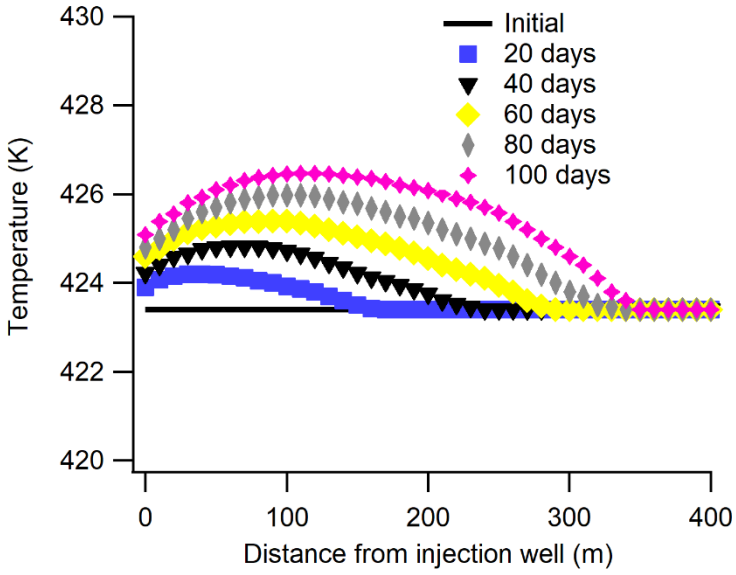

Figure 11. Temperature as a function of time and distance from the injection well (heat capacity of the reservoir, cap and base rocks set to 1500 $J.kg^{-1}.K^{-1}$ - end of injection: 300 days).

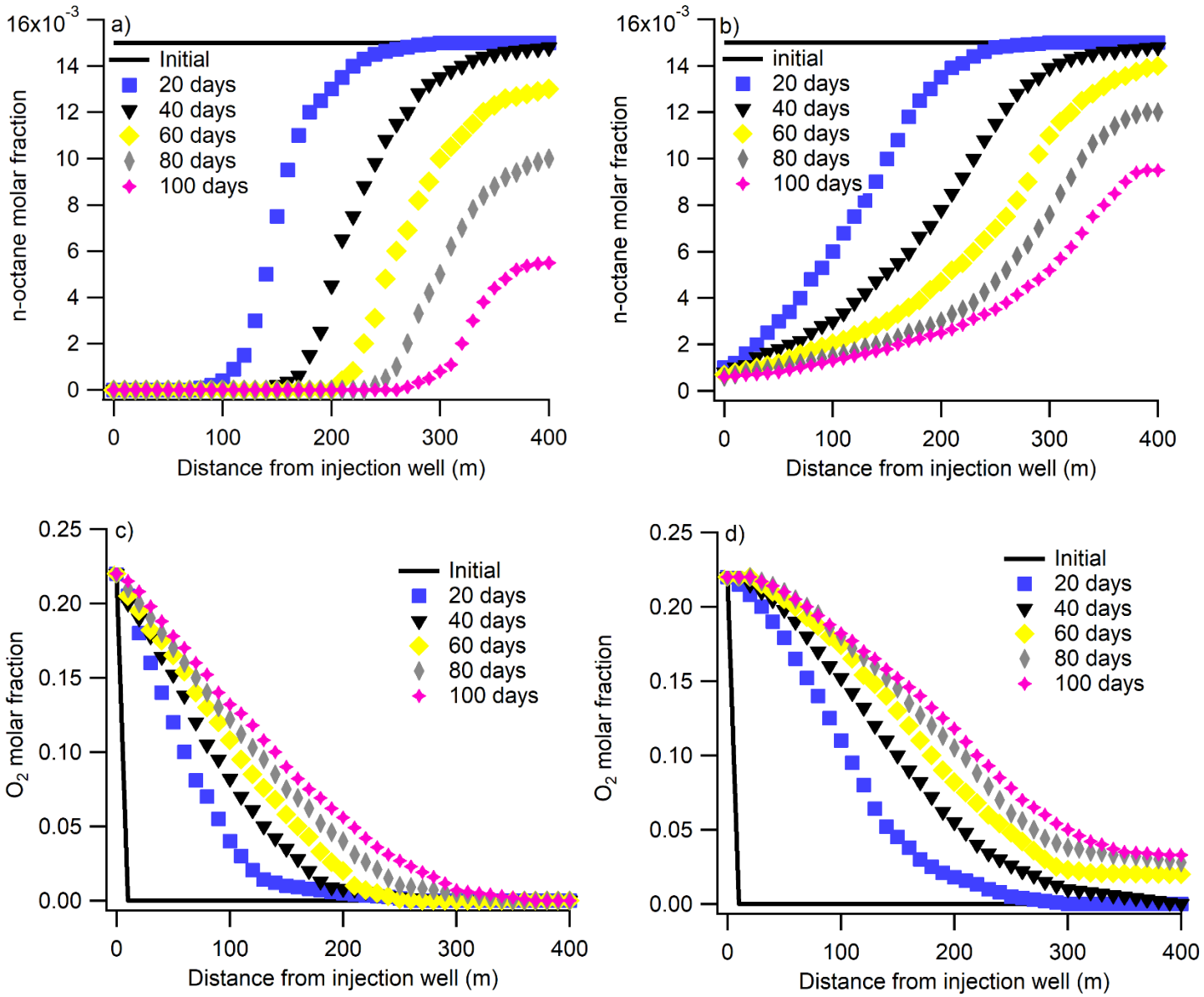

440

441 **Figure 12.** Reactant molar fractions as a function of time and distance from the injection well: a) *n*-
442 octane (reactant present in the reservoir) and heat capacity of the reservoir, cap and base rocks set to
443 500 J.kg^{-1}.K^{-1}; b) *n*-octane and heat capacity set to 1 500 J.kg^{-1}.K^{-1}; c) O_2 (injected into the reservoir) and
444 heat capacity set to 500 J.kg^{-1}.K^{-1}; d) O_2 (injected into the reservoir) and heat capacity set to 1 500 J.kg^{-}
445 ^{1}.K^{-1} (end of injection: 300 days).

446

447

4. Conclusions

The paper aimed at studying the influence of oxygen contained in the flue gas, for an example captured after oxy-combustion, on the oxidation kinetics of the residual fuel in the depleted reservoir and its influence on some of the reservoir parameters or properties. More precisely, the paper focused on the influence of the oxidation exothermicity and the thermal properties of the rocks on the pressure and the temperature evolution, and on the kinetics of the reaction inside a depleted oil reservoir.

Despite some assumptions and a quite high initial concentration of O_2, it clearly appears that the system is not inert with respect to the hydrocarbons reactivity. The residual oil is probably consumed in less than one year in relatively small reservoirs, leading to the temperature increase throughout the reservoir. After the end of the reaction, the temperature decreases slowly by heat dissipation in the cap and base rocks.

The extent of increase in the reservoir temperature is clearly a function of the thermal properties of the rocks. It has been demonstrated that the thermal conductivity of the rocks and their potential anisotropy have only a small influence on the temperature evolution. Nevertheless, the temperature evolution is highly dependent on the heat capacity and quite contrasting behaviors can be observed depending on low or high heat capacities of the rocks. A high heat capacity of the rock leads to a negligible increase in the temperature of the reservoir. Therefore, in order to limit the temperature increase and the kinetics of the reaction, it appears important to select reservoirs whose rocks as well as the rocks of the cap and the base have a high heat capacity (greater than 1000 $J.kg^{-1}.K^{-1}$), especially when O_2 concentration in the injected gas is high (at least greater than 3%). In this case, the temperature increase seems negligible and the oil oxidation is very slow, which appears to be an essential condition for a safe injection operation. Consequently, for a depleted reservoir with rocks of low heat capacity, it is important to decrease the O_2 concentration in the injected gas, its flow rate,

and the temperature and the pressure in the well, in order to limit the risk of significantly rapid rise in the reservoir temperature and its associated thermal instability issues.

This research did not receive any specific grant from funding agencies in the public, commercial, or not-for-profit sectors.

References

Ahmadi, M. A., Pouladi, B., Barghi, T., 2016. Numerical modeling of CO_2 injection scenarios in petroleum reservoirs: Application to CO_2 sequestration and EOR. Journal of Natural Gas Science and Engineering 30, 38-49. doi: 10.1016/j.jngse.2016.01.038

Arbogast, T., Douglas, J., Hornung, U., 1990. Derivation of the double porosity model of single-phase flow via homogenization theory. Siam J. Math. Anal. 21(4), 823-836. doi: 10.1137/0521046

Bender, S., Akin, S., 2017. Flue gas injection for EOR and sequestration: Case study. Journal of Petroleum Science and Engineering 157, 1033-1045. doi: 10.1016/j.petrol.2017.07.044

Birch, F., Clark, H., 1940. The thermal conductivity of rocks and its dependence upon temperature and composition. Part I. Am. J. Science 238(8), 529-558.

Bothe, D., 2011. On the Maxwell-Stefan approach to multicomponent diffusion. In: Escher J. et al. (eds) Parabolic Problems. Progress in Nonlinear Differential Equations and Their Applications, vol 80. Springer, Basel. doi: 10.1007/978-3-0348-0075-4_5

COMSOL Multiphysics® v.5.6. www.comsol.com. COMSOL AB, Stockholm, Sweden.

De Soete, G., Feugier, A., 1976. Aspects physiques et chimiques de la combustion. Ed. TECHNIP.

Fuller, E.N., Schettle, P.D., Giddings, J.C., 1966. A new method for prediction of binary gas-phase diffusion coefficients. Ind. Eng. Chem. 58(5), 18-27. doi: 19. 10.1021/ie50677a007

Garo, A., Puechberty, D., Ledoux, N., 1984. Recombination Kinetics of OH Radicals on a Quartz Wall in a Propane-Oxygen Flame at 25 Torr. Combust. Flame 56, 307-316. doi: 10.1016/0010-2180(84)90064-6

Girard, J-P., Chiquet, P., Thibeau, S., Lescanne, M., Prinet, C., 2013. Geochemical assessment of the injection of CO_2 into Rousse depleted gas reservoir. Part I: Initial mineralogical and geochemical conditions in the Mano reservoir. Energy Procedia 37, 6395 – 6401. doi: 10.1016/j.egypro.2013.06.569

Hamza, A., Hussein, I.A., Al-Marri M.J., Mahmoud, M., Shawabkeh, R., Aparicio, S., 2021. CO_2 enhanced gas recovery and sequestration in depleted gas reservoirs: A review. Journal of Petroleum Science and Engineering 196, 107685. doi: 10.1016/j.petrol.2020.107685

IEA, International Energy Agency, 2022. Data and Statistics [online] Available on: https://www.iea.org/data-and-statistics [accessed 11 February 2022]

IPCC, 2021: Climate Change 2021: The Physical Science Basis. Contribution of Working Group I to the Sixth Assessment Report of the Intergovernmental Panel on Climate Change [Masson-Delmotte, V., P. Zhai, A. Pirani, S.L. Connors, C. Péan, S. Berger, N. Caud, Y. Chen, L. Goldfarb, M.I. Gomis, M. Huang, K. Leitzell, E. Lonnoy, J.B.R. Matthews, T.K. Maycock, T. Waterfield, O. Yelekçi, R. Yu, and B. Zhou (eds.)]. Cambridge University Press. In Press.

Kaldi, J.G., Gibson-Poole, C.M., Payenberg, T.H.D., 2009. Geological input to selection and evaluation of CO_2 geosequestration sites. Carbon Dioxide sequestration in geological media - State of the science: AAPG Studies in Geology 59, 5 - 16. doi: 10.1306/13171230St59227

Kee, R.J., Rupley, F.M., Miller, J.A., 1989. CHEMKIN-II: A Fortran chemical kinetics package for the analysis of gas-phase chemical kinetics. Sandia Report, SAND-89-8009.

Kihm, J-H., Park, J-Y., Lee, S., Kim, J-M., Yum, B-W., 2019. Thermo-hydrological numerical evaluation of carbon dioxide injection efficiency for its geologic storage using a coupled reservoir-well simulation scheme. Int. J. Greenh. Gas Control 90, 102623. doi: 10.1016/j.ijggc.2019.01.012

Krupka, K.M., Hemingway, B.S., Robie, R.A., Kerrick, D.M., 1985. High-temperature heat capacities and derived thermodynamic properties of anthophyllite, diopside, dolomite, enstatite, bronzite, talc, tremolite, and wollastonite. American Minerogist 70, 261-271.

Liu, Y., Wang, P., Yang, M., Zhao, Y., Zhao, J., Song, Y., 2018. CO_2 sequestration in depleted methane hydrate sandy reservoirs. Journal of Natural Gas Science and Engineering 49, 428-434. doi: 10.1016/j.jngse.2017.10.023

528 Maroto-Valer, M.M. Developments and innovation in carbon dioxide (CO_2) capture and storage
529 technology. Volume 1: Carbon dioxide (CO_2) capture, transport and industrial applications. Woodhead
530 publishing series in energy: number 8, CRC Press, 2010.

531 Mikunda, T., 2012. CO_2 storage: Do impurities matter? Carbon capture J. April 27.

532 Monteiro, P. J. M., Rycroft, C.H., Barenblatt, G.I., 2012. A mathematical model of fluid and gas flow in
533 nanoporous media. Proc Natl Acad Sci USA 09(50), 20309–20313. doi: 10.1073/pnas.1219009109

534 Pacini-Petitjean, C, 2015. Réactivité des hydrocarbures en réponse à une injection de CO_2/O_2 dans des
535 conditions de réservoirs déplétés : modélisations expérimentale et numérique. PhD Thesis. Université
536 de Lorraine, France. [online] Available on: http://docnum.univ-
537 lorraine.fr/public/DDOC_T_2015_0020_PACINI_PETITJEAN.pdf

538 Pacini-Petitjean, C., Faure, P., Burklé-Vitzthum, V., Pironon, J., Randi, A., 2015a. Oxidation of *n*-
539 hexadecane and crude oil in context of gas mixture injection (CO_2/O_2) under depleted reservoir
540 conditions. Int. J. Greenh. Gas Control, 35, 110-119. doi: 10.1016/j.ijggc.2014.12.024

541 Pacini-Petitjean, C., Morajkar, P., Burklé-Vitzthum, V., Randi A., Lorgeoux C., Morel, D., Pironon, J.,
542 Faure, P, 2015b. Oxidation of n-alkane (n-C_8H_{18}) under reservoir conditions, in context of gas mixture
543 injection (CO_2/O_2): Construction of a kinetic model. Energy Fuels 29, 1912-1922. doi:
544 10.1021/ef502553x

545 Pacini-Petitjean, C., Morajkar, P., Burklé-Vitzthum, V., Randi, A., Lorgeoux, C., Morel, D., Pironon, J.,
546 Faure, P, 2016. Oxidation of n-alkane (n-C_8H_{18}) under reservoir conditions, in context of gas mixture
547 injection (CO2/O2): Understanding of oxygenated compounds distribution. Energy Fuels, 30, 7560-
548 7570. doi: 0.1021/acs.energyfuels.6b01323

549 Renard, S., Sterpenich, J., Pironon, J., Chiquet, P., Randi, A., 2014. Geochemical effects of an
550 oxycombustion stream containing SO_2 and O_2 on carbonate rocks in the context of CO2 storage.
551 Chemical Geology, 382, 140–152. doi: 10.1016/j.chemgeo.2014.05.032

552 Sutherland, W., 1893. The viscosity of gases and molecular force. London Edinburgh Dublin Philos.
553 Mag. J. Sci. 36, 507-531. doi.org/ 10.1080/14786449308620508

554 Tumsa, T.Z., Mun, T-Y., Lee, U., Yang, W., 2017. Effects of coal characteristics to performance of a highly
555 efficient thermal power generation system based on pressurized oxy-fuel combustion. Int. J. Energy
556 Res. 41, 127-138. doi: 10.1002/er.3608

557 Turns, S. R., 2012. An Introduction to Combustion: Concepts and Applications. 3rd ed., New York:
558 McGraw-Hill.

559 Wang, J., Ryan, D., Anthony, E., Wingston, A., Basava-Reddi, L., Wildgust, N., 2012. The effect of
560 impurities in oxyfuel flue gas on CO_2 storage capacity. Int. J. Greenh. Gas Control, 11, 158-162. doi:
561 10.1016/j.ijggc.2012.08.002

562 Wesselingh, J.A, Krishna, R., 2000. Mass Transfer in Multicomponent Mixtures. Delft University Press.

563 Yucel Akkutlu I., Yortsos Y.C., 2003. The dynamics of in-situ combustion fronts in porous media.
564 Combust. Flame 134, 229-247. doi: 10.1016/S0010-2180(03)00095-6

565 Zhang, X., Ranjith, P.G., 2019. Experimental investigation of effects of CO_2 injection on enhanced
566 methane recovery in coal seam reservoirs. Journal of CO_2 Utilization 33, 394-404. doi:
567 10.1016/j.jcou.2019.06.019

568

569

570